THE AMERICAN SOCIETY OF MECHANICAL ENGINEERS
Three Park Avenue, New York, N.Y. 10016-5990

99-GT-137

THE EFFECT OF SCHMIDT NUMBER ON TURBULENT SCALAR MIXING IN A JET-IN-CROSSFLOW

Guangbin He, Yanhu Guo, and Andrew T. Hsu
University of Miami
Department of Mechanical Engineering
Coral Gables, Florida 33124
Tel: 305-284-4806
Fax: 305-284-2580
E-mail: ghe@coeds.eng.miami.edu

A. Brankovic and S. Syed
Pratt & Whitney
West Palm Beach, FL 33410

N.-S. Liu
NASA Lewis Research Center
Cleveland, OH 44135

ABSTRACT

The adequacy and accuracy of the constant Schmidt number assumption in predicting turbulent scalar fields in jet-in-crossflows are assessed in the present work. A round jet injected into a confined crossflow in a rectangular tunnel has been simulated using the Reynolds-Averaged Navier-Stokes equations coupled with the standard k-ε turbulence model. A semi-analytical qualitative analysis was made to guide the selection of Schmidt number values. A series of parametric studies were performed, and Schmidt numbers ranging from 0.2 to 1.5 and jet-to-crossflow momentum flux ratios from 8 to 72 were tested. The principal observation is that the Schmidt number does not have an appreciable effect on the species penetration, but it does have a significant effect on species spreading rate in jet-in-crossflows, especially for the cases where the jet-to-crossflow momentum flux ratios are relatively small. A Schmidt number of 0.2 is recommended for best agreement with data. The limitations of the standard k- ε turbulence model and the constant Schmidt number assumption are discussed.

NOMENCLATURE

A_j	= Jet exit area
D	= Jet diameter
D_ϕ	= Turbulent diffusion coefficient
H	= Tunnel height
J	= Jet-to-crossflow momentum flux ratio
k	= Turbulence kinetic energy
Pe	= Peclet number
Sc	= Turbulent Schmidt number
T	= Temperature
U, V, W	= Mean velocity components in Cartesian coordinates
X, Y, Z	= Cartesian coordinates
ε	= Dissipation rate of the turbulence kinetic energy
ϕ	= General dependent variable
ν	= Molecular viscosity
ν_e, ν_t	= Effective and eddy viscosity, respectively
θ	= Non-dimensional temperature
ρ	= Density

1. INTRODUCTION

Jet-in-crossflows are extensively used in gas turbine combustors, where jets are arranged around the circumference of combustion chambers to enhance combustion performance in the primary zone and to dilute the hot combustion product exiting the combustor. For modern low-emission gas turbine combustors, the distributions of temperature and species concentration at the combustor exit are important design parameters. Therefore, quantitative predictions of both species and temperature distributions downstream of the jet are required for advanced combustor design.

The flow configurations of jet-in-crossflow problems generally include single and multiple jets in a crossflow. A large body of experimental and computational results of multiple jets a crossflow has been obtained by Holdeman et al.

Presented at the International Gas Turbine & Aeroengine Congress & Exhibition
Indianapolis, Indiana — June 7–June 10, 1999

(1993 and 1997) and Liscinsky et al. (1993-1996). In the current literature review, we limit the scope on the flow configuration of a single round jet normally into a confined rectangular duct.

Many researchers have experimentally studied a single round jet normally into a confined rectangular crossflow. The majority of past experimental work concentrate on trying to understand the flow structures and velocity field of jet-in-crossflows (see, e.g., Crabb, et al. 1981, Andreopoulos & Rodi, 1984, Fric & Roshko, 1994, Kelso et. al., 1996). Compared to velocity measurements and flow structure studies, the experimental work on scalar diffusion in jet-in-crossflows are relatively few. Kamotani and Greber (1972 and 1974) studied the scalar diffusion problem using a heated air jet injected into crossflow, where temperature distribution downstream of the jet was measured using hot wire. Sherif and Pletcher (1989) measured the temperature field of a heated water jet normally injected into a water tunnel. Vranos and Liscinsky (1988) used marker nephelometry to measure the mean concentration in the center plane of a single jet in crossflow; the results were in good agreement with the single-point measurements of Kamotani and Greber (1972). More recently, laser induced fluorescence has been used to measure the whole flowfield using dye as a scalar tracer. Smith and Mungal (1998) used acetone vapor seeded into the jet to acquire quantitative two-dimensional images of the scalar concentration field for a wide range of velocity ratios.

Numerical simulations of the jet-in-crossflow problem include mainly two groups of approaches: the first employs Direct Numerical Simulation (DNS) or Large-Eddy Simulation (LES), and the second uses the Reynolds averaged approach. Hahn and Choi (1997) used DNS to study the flow structure and velocity field of the jet-in-crossflow at very low Reynolds numbers and low jet-to-crossflow momentum flux ratios. Yuan (1997) used LES method to simulate both the velocity field and scalar transport of the Sherif and Pletcher (1989) case at reduced Reynolds numbers. Although DNS and LES has shown promising results, they are not at this point employed by the aircraft engine industry in their routine design simulations because of the relatively large computer memory and CPU requirement.

In current design practices, Reynolds-Averaged Navier-Stokes (RANS) computations are most often used for investigation of the velocity and combustion field of gas turbine combustors. Therefore, there is a need for accurate RANS simulations of the jet-in-crossflow problem; both the prediction of velocity field and the scalar field are desired. RANS simulation of the velocity field has been performed by many researchers in the past (see, e.g., Patankar et al. 1977, Claus & Vanka, 1992, Kim & Benson 1992). By contrast numerical simulations of scalar diffusion in jet-in-crossflows are relatively few, and no systematic study of the Schmidt number effects is available. Chao and Ho (1990) used RANS and the standard k-ε model to calculate the temperature field that was experimentally measured by Kamotani and Greber (1974), and found no significant changes in the temperature contour patterns when Schmidt numbers ranging from 0.5 to 0.9 were used. Catalano et al. (1989) predicted the scalar field of a flow where the jet impinged on the ceiling wall but did not mention the value or the effect of the Schmidt number. More recently, Gulati et al. (1994) found that a Schmidt number of 0.25 is an appropriate value used in practice to match the pattern factor at the combustor exit.

The present work focuses on the numerical simulation of turbulent scalar transport in jet-in-crossflows. The objective is to evaluate the accuracy and limitations of the constant Schmidt number assumption, and to give recommendations on the Schmidt number values most suitable for jet-in-crossflow simulations. A semi-empirical analysis on the Schmidt number is first carried out to provide guidance for later numerical studies. A series of RANS simulations, using Schmidt numbers ranging from 0.2 to 1.5, of a confined jet-in-crossflow is performed, wherein turbulence closure is provided by a standard k-ε model. The flow configuration studied in the present work is a round turbulent jet discharging normally into a uniform crossflow in a rectangular tunnel, which was experimentally investigated by Crabb et al. (1981) and Kamotani & Greber (1974). The experimental data from these two groups are used to calibrate the Schmidt number selections.

2. COMPUTATIONAL APPROACH

2.1 Governing Equations

For a variable density incompressible steady flow with constant viscosity, the Reynolds-averaged governing equations for mass, momentum, turbulent kinetic energy and its dissipation rate (the standard k-ε model, Launder & Spalding, 1974), and species concentration, can be written in the following general form:

$$\frac{\partial}{\partial x_j}(\rho U_j \phi) = \frac{\partial}{\partial x_j}\left(D_\phi \frac{\partial \phi}{\partial x_j}\right) + S_\phi \qquad (1)$$

where

$$D_\phi = \frac{\nu_e}{Sc_\phi} \qquad (2)$$

is the diffusion coefficient; ϕ is the dependent variable, such as velocity, turbulent kinetic energy, dissipation rate, and species concentration; Sc_ϕ represents the turbulent Prandtl or Schmidt number; ν_e is the effective viscosity that is equal to the sum of turbulent viscosity ν_t and molecular viscosity ν; and S_ϕ is the source term.

Since the governing equation for species concentration is identical to the equation for enthalpy if there are no chemical

reactions and no external heat source in the physical domain considered, the equation for enthalpy was used throughout the present study, and Schmidt number and Prandtl number were not distinguished.

2.2 Numerical Schemes

A hybrid differencing scheme and a second-order upwind differencing scheme (Zhu, 1991) are used in the discretization of the above differential equations. The computational node locations are shown in Fig. 1. The governing equations are discretized using the finite volume scheme on a given cell, P. In evaluating the fluxes on the cell surfaces, the primitive variable ϕ at a surface (e.g., west surface) of a control volume is calculated using the following scheme.

$$\phi_w = \phi_W + \gamma_w(\phi_P - \phi_W)\frac{\phi_W - \phi_{WW}}{\phi_P - \phi_{WW}} \tag{3}$$

where

$$\gamma_w = \begin{cases} 1 & if \left|\dot{\phi}_W - 0.5\right| < 0.5 \\ 0 & otherwise \end{cases} \tag{4}$$

and

$$\dot{\phi}_W = (\phi_W - \phi_{WW})/(\phi_P - \phi_{WW}) \tag{5}$$

Because the above second-order differencing scheme requires two upstream nodes for each cell-face, which will involve a value outside the solution domain for a near-boundary control volume, the following Hybrid scheme was used for all the control volumes adjacent to boundaries.

$$\phi_w = \begin{cases} 0.5(\phi_P + \phi_W) & if \quad Pe \le 2 \\ \phi_W & otherwise \end{cases} \tag{6}$$

where Pe is the Peclet number, defined as

$$Pe = \left|C_w / D_w\right| \tag{7}$$

with C_w representing the mass flux across the west surface and D_w representing the conductance coefficient at the west surface.

The Semi-Implicit Method for Pressure-Linked Equations (SIMPLE) (Patankar & Spalding, 1972) algorithm was used to handle the pressure-velocity coupling. In order to stabilize the solution, under-relaxation factors were used for primitive variables.

2.3 Boundary Conditions

A uniform velocity profile at the crossflow inlet was assumed. The velocity profile of a fully developed turbulent pipe flow was used at the jet inlet boundary. No-slip condition was imposed on the walls, and the standard wall function (Launder & Spalding, 1974) was used with the standard k- ε model. At the inlets of the jet and the crossflow, the turbulence kinetic energy k and its dissipation rate ε are calculated as

$$k = a(U^2 + V^2 + W^2) \tag{8}$$

$$\varepsilon = \frac{C_\mu \rho k^2}{b\mu} \tag{9}$$

where a is a constant, b is the ratio of μ_t/μ. In our calculations, a=0.005 and b=100. A zero gradient condition on all flow variables was imposed at the outflow boundary.

2.4 Flow Configuration and Grid

As mentioned in the introduction, the flow configuration used in this work is that of a round turbulent jet normally discharging into a uniform crossflow. In the case of Crabb et al., a turbulent jet was injected normally into a uniform mainstream in a rectangular wind tunnel from a 25.4mm inside diameter and 0.75m long pipe. The jet-to-crossflow velocity ratio is 2.3, the crossflow velocity is 12.0 m/s. The jet and the crossflow have the same temperature. A laser Doppler anemometer (LDA) was used to measure the velocity field.

In the case of Kamotani & Greber, a heated round jet was issued normally into a uniform crossflow in a rectangular tunnel. The temperature difference between the jet and the crossflow is 167°K, with the jet temperature at 465°K. Iron-constantan thermocouples were used to measure the temperature distribution. The distance from the jet exit to the ceiling wall is H=12D for momentum flux ratios of J=8 and 32, and H=24D for J=72. The jet-to-crossflow momentum flux ratio is defined as:

$$J = \frac{\int_{A_j} \rho_j V_j^2 dA}{\rho_o U_o^2 A_j} \tag{10}$$

where U_o is crossflow velocity, V_j is jet velocity, A_j is the jet area, ρ is density, subscripts o and j denote crossflow and jet, respectively.

Based on the symmetry about the jet center plane, the computational domain was established on half the flowfield. The flow geometry and the coordinate system are described in the Fig. 2. The jet center is located at 6D downstream of the crossflow inlet, which guarantees that the inlet boundary of the crossflow has little effect on the computed flowfield. In order to eliminate any unwanted feedback from the downstream boundary, the tunnel exit is put at 29D downstream of the jet. The domain size in the spanwise and the vertical direction are 8D and 12D, respectively. In this computation domain, a nonorthogonal boundary-fitted grid of 90x45x40 was generated in the streamwise, vertical, and spanwise direction, respectively. This selection is the result of a grid dependency

study, where grid sizes of 50x40x30, 70x45x40, 90x45x40, and 90x50x40 have been tested, together with various stretching factors. As shown in Fig. 3, stretched grids were used along the streamwise and spanwise direction, while uniform grids were used along the vertical direction. 10 uniform grids were selected inside the jet in the streamwise direction as a result of grid independence study.

3. QUALITATIVE ANALYSES FOR SELECTION OF SCHMIDT NUMBER

In order to provide some theoretical guidance in the selection of Schmidt numbers, the following analysis is done based on empirical correlations given by Kamotani & Greber (1972).

Kamotani and Greber established correlations of the velocity and temperature trajectories based on their experimental data:

$$\frac{y_v}{D} = a_v\left(\frac{x}{D}\right)^{b_v} \tag{11}$$

$$\frac{y_T}{D} = a_T\left(\frac{x}{D}\right)^{b_T} \tag{12}$$

where y_v and y_T denote vertical coordinates of velocity trajectory and temperature trajectory, respectively; a_v, b_v, b_T are functions of the jet-to-crossflow momentum flux ratio and a_T depends mainly upon the momentum flux ratio and weakly upon the density ratio. With the momentum flux ratio in the range of 15 to 60, and the temperature difference in the range of 0°K to 177°K, the above two formulas become

$$\frac{y_v}{D} = 0.89J^{0.47}\left(\frac{x}{D}\right)^{0.36} \tag{13}$$

$$\frac{y_T}{D} = 0.73J^{0.52}\left(\frac{\rho_j}{\rho_o}\right)^{0.11}\left(\frac{x}{D}\right)^{0.29} \tag{14}$$

where J is the jet-to-crossflow momentum flux ratio, ρ_j and ρ_o are densities of the jet and the crossflow. One may assume a relation between the turbulent Schmidt number and the trajectories of the velocity and the temperature by using Eqs. (13) and (14).

$$Sc_\phi = \frac{\nu_t}{D_\phi}$$

$$\propto \frac{y_T}{y_v} = 0.82J^{0.05}\left(\frac{\rho_j}{\rho_o}\right)^{0.11}\left(\frac{x}{D}\right)^{-0.07} \tag{15}$$

The above empirical relationship indicates that the turbulent Schmidt number increases slightly with increasing momentum flux ratio and density ratio, and decreases with increasing x/D. This argument gives a qualitative guide for selection of Schmidt number in the following jet-in-crossflows simulations.

4. COMPUTATIONAL RESULTS AND DISCUSSION

In this section, we present the computed results of mean velocity, turbulence intensity, jet trajectories, and temperature contours. These calculated results are compared with experimental measurements of Crabb et al. (1981) and Kamotani & Greber (1974). The limitations of the constant Schmidt assumption and k-ε model in scalar predictions are discussed.

In all the computations reported in the following, a grid of 90x45x40 was used and a grid dependence study found that further refinement of the grid did not affect the solution. Convergence was determined by monitoring the L2-norm of the flux residuals. To get converged solutions, the residuals dropped at least 3 orders of magnitude for velocity components and at least 2 orders for scalar variables. Figure 4 shows a typical convergence history. 350 iterations were generally required for the cases where Schmidt numbers are relatively high (greater than 0.5), and 450 or more iterations were required for the low Schmidt number cases (Sc=0.2 and 0.3). A converged solution required approximately 220μs/iteration/grid-point CPU time on an SGI-OCTANE workstation, and required approximately 350 μs/iteration/grid-point CPU time on an SGI-INDY workstation.

4.1 Mean Velocity and Turbulence Intensity Calculations.

Comparisons of the calculated velocities with experimental data of both Crabb at al. and Kamotani & Greber are shown in Fig. 5. Figure 5 (a) presents the streamwise velocity distribution at the jet center plane and y=1.35D, and Figure 5(b) presents the comparison at the jet center plane and x=8D for the case of Crabb et al. Figure 5 (c) shows the predicted streamwise velocity at the jet center plane and x=12D for the case of J=32, compared to the measured velocity by Kamotani & Greber (1974). Figure 6 compares the computed turbulence intensity with experimental data at the jet center plane and y=1.35D for the case of Crabb et al. The calculated results of Claus & Vanka (1992) using 2.4 million computational nodes, are also presented in the same figure.

Figures 5 and 6 show that although the velocity fields were reasonably well predicted, but the turbulence intensity was somewhat under-predicted. The discrepancies between numerical predictions and experimental data are believed to be caused by the deficiencies of the standard k-ε model. The standard k-ε model is strictly based on a gradient hypothesis for the turbulent fluxes. Andreopoulos and Rodi (1984) had shown experimentally that there is a significant counter

gradient transport in the jet-in-crossflow configuration, which points to the inadequacy of the standard k- ε model in jet-in-crossflow simulations.

4.2 Jet Temperature Trajectories.

Jet trajectory is one of the most important characteristics of jet-in-crossflow problems. The jet temperature trajectory is defined as the locus of the local maximum temperature. The numerically predicted jet trajectories are compared with experimental data of Kamotani & Greber (1974) in Figs. 7 and 8. Figure 7 presents the solutions obtained using various Schmidt numbers compared with experimental data for the case of J=32. The trajectories obtained using Schmidt numbers ranging from 0.2 to 1.5 all have fairly good agreement with experimental data, which indicates that Schmidt number has very little effect on the prediction of the jet trajectory. Figure 8 shows the predicted jet trajectories using a Schmidt number of 0.5 for the cases of J=8, 32 and 72 compared with the experimental results. General agreement is observed.

4.3 Non-Dimensional Temperature Contours.

The temperature was non-dimensionalized by

$$\theta = \frac{T - T_o}{T_j - T_o} \tag{16}$$

where T_j is temperature of the jet and T_o is temperature of the crossflow.

The temperature contours at the jet center plane for various momentum flux ratios are compared with experimental data in Figs. 9, 10, and 11.

Momentum flux ratio J=8.

Schmidt numbers 0.2, 0.3, 0.5, 0.8, and 1.2 were tested to study the effects of Schmidt number on the jet mixing in the crossflow for the case of J=8.

Figure 9 shows a quantitative comparison of the numerically predicted temperature contours with experimental results. Figure 9(a) presents the experimental measurements of the temperature distribution in the jet center plane, and Figures 9(b) through 10(f) are numerical results from various Schmidt numbers. These results show that the temperature profiles become slenderer with increasing Schmidt number. For example, the contour line of θ=0.1 was predicted to be x=10D downstream of the jet exit when a Schmidt number of 0.2 was used (Fig. 9(b)), while as shown in Fig. 9(d), the location of the contour line of θ=0.1 extended to x=20D when a Schmidt number of 0.5 was used. The jet mixing rate was found to be quite sensitive to the change in Schmidt number for this low momentum flux ratio; the predicted temperature field changes substantially with the Schmidt number. In fact, when the Schmidt number is greater than 0.3, the agreement between predicted and measured temperature fields become poor.

It should be noted that although the best agreement with experimental data is obtained with Sc=0.2, the agreement with experimental data is far from perfect. For instance, the lower part of the contour line of θ=0.025, observed in the experimental data as shown in Fig. 9(a), was not resolved in the prediction using Sc=0.2 (Fig. 9(b)). An increase or decrease in the Schmidt number from the 0.2 value will improve the temperature prediction in some regions but worsen it in others. This indicates that, for low jet-to-crossflow momentum flux ratios, the assumption of a constant Schmidt number may not be the best choice for the jet-in-crossflow problem, and more sophisticated approaches may be required.

Momentum flux ratio J=32.

Schmidt numbers tested for the case of J=32 were Sc=0.2, 0.3, 0.5, and 0.7. Figure 10(a) presents the experimental measurements, and Figures 10(b) through 10(e) show numerical results from various Schmidt numbers. In this case, the jet impinged upon the ceiling wall at the downstream of the jet. Generally, a Schmidt number of 0.2 still gives the best agreement with experimental data. The jet scalar diffusion is under-predicted with Schmidt numbers greater than 0.3, but the change is less significant than in the case of J=8. Compared to the case of J=8, the present results show much better agreement with experimental data.

Momentum flux ratio J=72.

Schmidt numbers 0.2, 0.3, 0.5 and 0.8 were used in the case of J=72. Results are presented in Fig. 11. It can be seen that the temperature field is quite accurately predicted at Sc=0.3. A close examination of Fig. 11 shows that the numerical results from Sc=0.2 also compare favorably with the experimental data of the temperature field, although scalar diffusion is slightly over-predicted.

A comparison of Figs. 9, 10, and 11 shows that the change in temperature distribution for J=72 with different Schmidt numbers is far less drastic compared to the cases of J=8 and 32. For the relatively high momentum flux ratio of J=72, the predicted temperature contours compare much better with experimental data than the two previous cases. One may conclude from this observation that the higher the jet-to-crossflow momentum flux ratio, the less sensitive is the solution to Schmidt number. One may also conclude that the constant Schmidt number assumption is a reasonable one for jet-in-crossflows of high jet-to-crossflow momentum flux ratios, but less so for those of low momentum flux ratios.

5. CONCLUDING REMARKS

RANS simulations of the turbulent scalar diffusion process in jet-in-crossflows were performed to evaluate the accuracy of constant Schmidt number assumption and the effect of Schmidt number on the mixing of jet species with the crossflow within the context of the standard k- ε model. Good prediction of the jet trajectories and reasonable prediction of the velocity field were obtained. Calculations showed under-predicted turbulence intensity, which indicates that the standard k- ε model does not capture all the important flow physics in jet-in-crossflows.

The Schmidt number does not have any appreciable effect on the jet trajectories but has significant effect on the rate of scalar mixing in the jet-in-crossflow, especially for cases where the jet-to-crossflow momentum flux ratios are relatively small. The most suitable Schmidt numbers for cases of J=8, 32, and 72 were found to be Sc=0.2, 0.2, and 0.3, which are considerably smaller than the values that are conventionally used in turbulent combustion simulations. A Schmidt number of 0.2 is recommended for jet-in-crossflow simulations because, under the constant Schmidt assumption, it gives the most satisfactory solutions for a wide range of jet-to-crossflow momentum flux ratios.

The constant Schmidt number assumption provides fairly accurate solutions of turbulent scalar mixing for jet-in-crossflow cases where the jet-to-crossflow momentum flux ratios are relatively high, while for low momentum flux ratio jet-in-crossflows a constant Schmidt number may not necessarily be the best choice. Our semi-empirical analysis based on the experimental observations of Kamotani & Greber, shows that the Schmidt number is dependent on the jet-to-crossflow momentum flux ratio, density ratio, and geometric location. From these observations one may conclude that a variable Schmidt number is needed for low momentum flux ratio jet-in-crossflows.

REFERENCES

Andreopoulos, J. and Rodi, W., 1984, "Experimental Investigation of Jets in a Crossflow", *Journal of Fluid Mechanics*, Vol. 138, pp. 93-127.

Catalano, G. D., Chang, K. S. and Mathis, J. A., 1989, "Investigation of Turbulent Jet Impingement in a Confined Crossflow", *AIAA Journal*, Vol. 27, No. 11, pp. 1530-1535.

Chao, Y. –C. and Ho, W. -C., 1990, "Heterogeneous and Non-isothermal Mixing of a Lateral Jet with a Swirling Crossflow", *Journal of Thermophysics*, Vol. 5, pp. 394-400.

Claus, R. W. and Vanka, S. P., 1992, "Multigrid Calculations of a Jet in Crossflow", *Journal of Propulsion and Power*, Vol. 8, No. 2, pp. 425-431.

Crabb, D., Durao, D. F. G. and Whitelaw, J. H., 1981, "A Round Jet Normal to a Crossflow", *Transactions of the ASME, Journal of Fluids Engineering*, Vol. 103, pp. 142-153.

Fric, T. F. and Roshko, A., 1994, "Vortical Structure in the Wake of a Transverse Jet", *Journal of Fluid Mechanics*, Vol. 279, pp. 1-47.

Gulati, A., Tolpaddi, A., and Vandeusen, G. et al., 1994, "Effect of Dilution air on Scalar Flowfield at Combustor Exit", AIAA, the 32nd Aerospace Sciences Meeting, Reno, Nevada, AIAA Paper 94-0221.

Hahn, S. and Choi, H., 1997, "Unsteady Simulation of Jets in a Cross Flow", *Journal of Computational Physics*, Vol. 134, pp. 342-356.

Holdeman, J. D., Liscinsky, D. S., and Bain, D. B., 1997, "Mixing of Multiple Jets with a Confined Subsonic Crossflow, Part II: Opposed Rows of Orifices in Rectangular Ducts", NASA Technical Memorandum 107461, ASME-97-GT-439.

Holdeman, J., D., 1993, "Mixing of Multiple Jets with a Confined Subsonic Crossflow", *Prog. Energ Combus. Sci.*, Vol. 19, pp. 31-70.

Kamotani, Y. and Greber, I., 1972, "Experiments on a Turbulent Jet in a Cross Flow", *AIAA Journal*, Vol. 10, No. 11, pp. 1425-1429.

Kamotani, Y. and Greber, I., 1974, "Experiments on Confined Turbulent Jets in Crossflow", NASA CR-2392.

Kelso, R. M., Lim, T. T., and Perry, A. E., 1996, " An Experimental Study of Round Jets in Crossflow", *Journal of Fluid Mechanics*, Vol. 306, pp. 111-114.

Kim, S. –W. and Benson, T. J., 1992, "Calculation of a Circular Jet in Crossflow with a Multiple-Time-Scale Turbulence Model", *Journal of Heat and Mass Transfer*, Vol. 35, No. 10, pp. 2357-2365.

Launder, B. E., and Spalding, D. B., 1974, "The Numerical Computation of Turbulent Flows", *Computer Methods in Applied Mechanics and Engineering*, Vol. 3, pp. 269-289.

Liscinsky, D. S., Vranos, A., and Lohmann, R. P., 1993, "Experimental Study of Cross Flow Mixing in Cylindrical and Rectangular Ducts", NASA Contractor Report 187141.

Liscinsky, D. S., True, B., and Holdeman, J. D., 1994, "Mixing Characteristics of Directly Opposed Rows of Jets Injected

Normal to a Crossflow in a Rectangular Duct", NASA Technical Memorandum 106477, AIAA-94-0217.

Liscinsky, D. S., True, B., and Holdeman, J. D., 1995, "Effects of Initial Conditions on a Single Jet in Crossflow", NASA Technical Memorandum 107002, AIAA-95-2998.

Liscinsky, D. S., True, B., and Holdeman, J. D., 1996, "Crossflow Mixing of Noncircular Jets", *Journal of Propulsion and Power*, Vol. 12, No. 2, pp. 225-230.

Patankar, S. V. and Spalding, D. B., 1972, " A Calculation Procedure for Heat, Mass and Momentum Transfer in Three-Dimensional Parabolic Flows", *International Journal of Heat and Mass Transfer*, Vol.15, pp. 1778-1806.

Patankar, S. V., Basu, D. K., and Alpay, S. A., 1977, "Prediction of the Three-Dimensional Velocity Field of a Deflected Turbulent Jet", *Transactions of the ASME, Journal of Fluid Engineering*, pp. 758-762.

Sherif, S. A. and Pletcher, R. H., 1989, "Measurements of the Thermal Characteristics of Heated Turbulent Jets in Crossflow", *Journal of Heat Transfer*, Vol. 111, pp. 897-903.

Smith, S. H. and Mungal, M. G., 1998, "Mixing, Structure and Scaling of the Jet in Crossflow", *Journal of Fluid Mechanics*, Vol. 357, pp. 83-122.

Vranos, A. and Liscinsky, D. S., 1988, "Planar Imaging of Jet Mixing in Crossflow", *AIAA Journal*, Vol. 26, pp. 1297-1298.

Yuan, L. L., 1997, "Large Eddy Simulations of a Jet in Crossflow", Ph. D. Dissertation, Stanford University.

Zhu, J., 1991, "FAST-2D: A Computer Program for Numerical Simulation of Two-Dimensional Incompressible Flows with Complex Boundaries", Report No. 690, Institute for Hydromechanics, University of Karlsruhe.

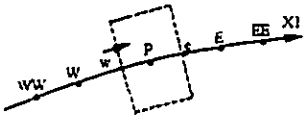

Fig. 1 Computational nodes.

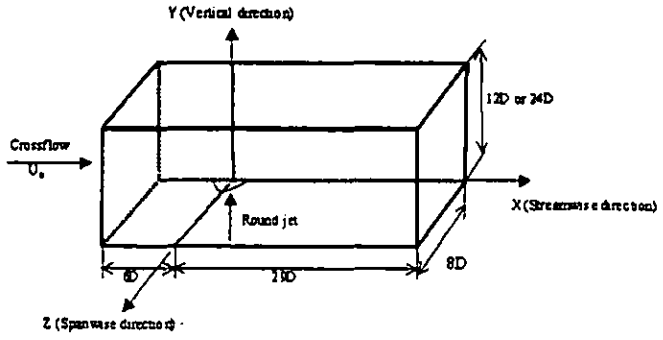

Fig. 2 Flow configuration and coordinate system.

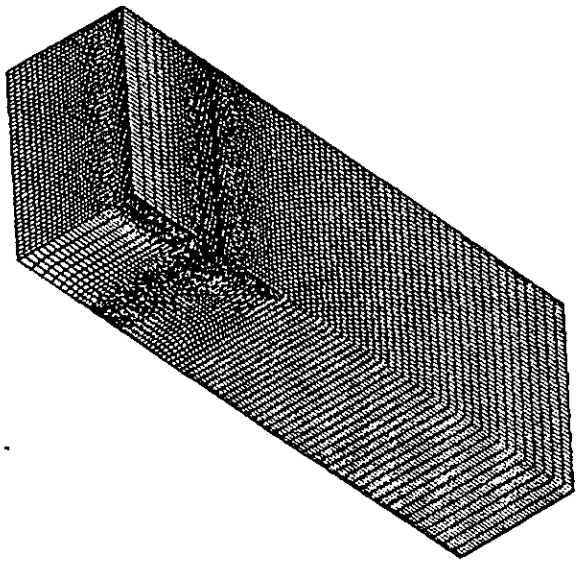

Fig. 3 Structured grid used in the current study.

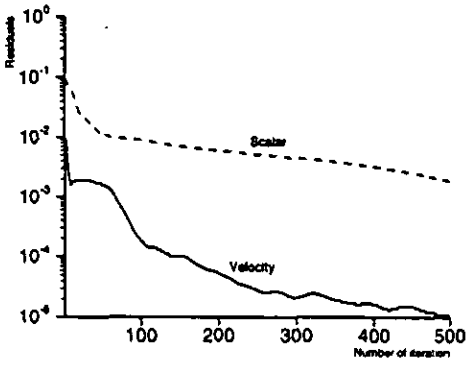

Fig. 4 Error residuals reducing history in the numerical solution.

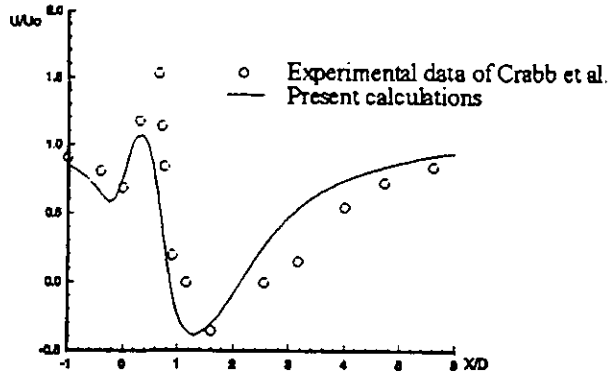

5(a) Y/D=1.35

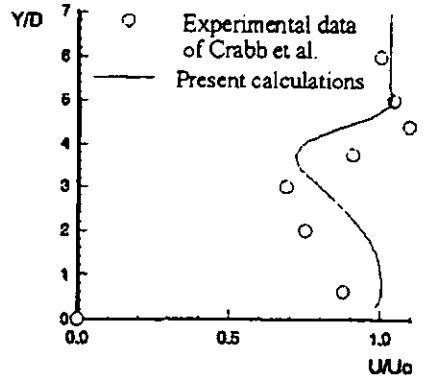

5(b) X/D=8

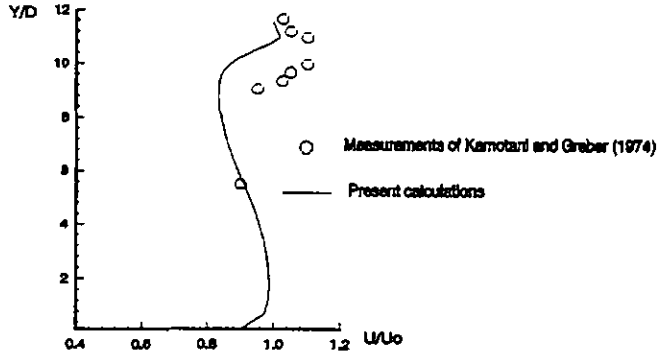

5(c) X/D=12

Fig. 5 Comparisons of predicted velocities with experimental data at the jet center plane.

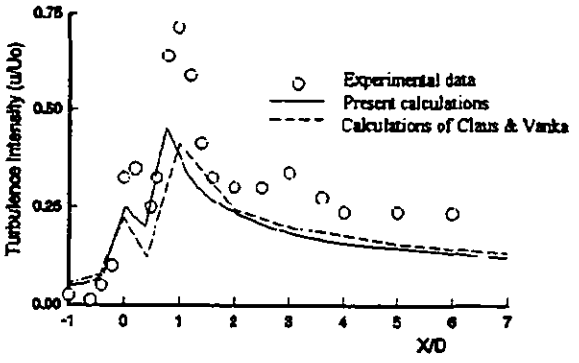

Fig. 6 Turbulence intensity at y/D=1.35 and Z/D=0, compared to the data of Crabb et al. (1981).

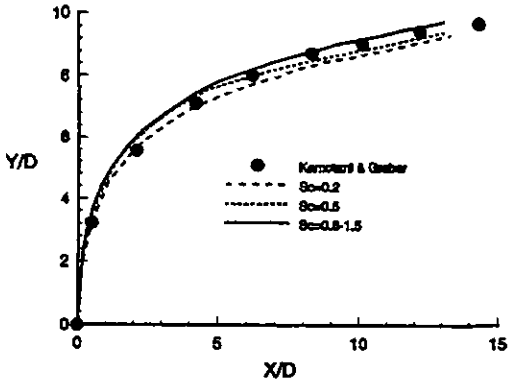

Fig. 7 Effect of Schmidt number on the jet temperature trajectory.

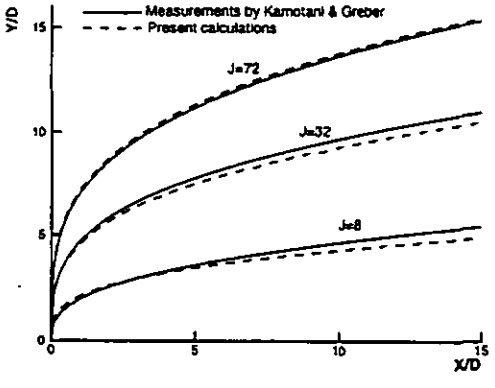

Fig. 8 Comparison of jet temperature trajectories between measurements and calculations.

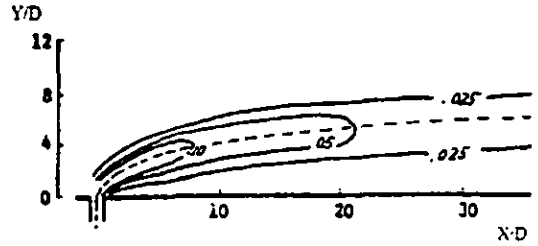

9(a) Experimental data

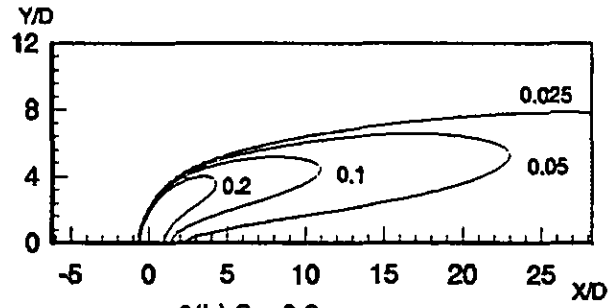

9(b) Sc=0.2

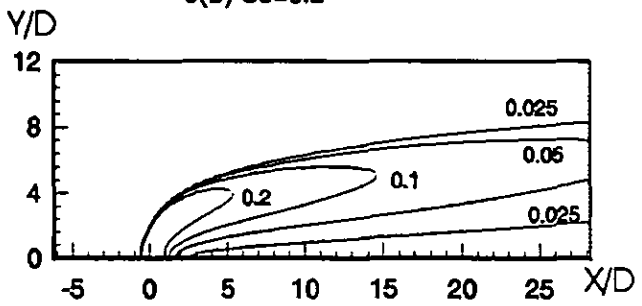

9(c) Sc=0.3

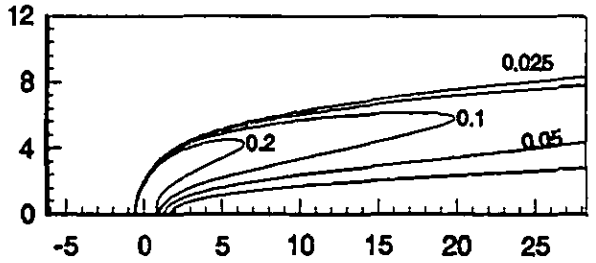

9(d) Sc=0.5

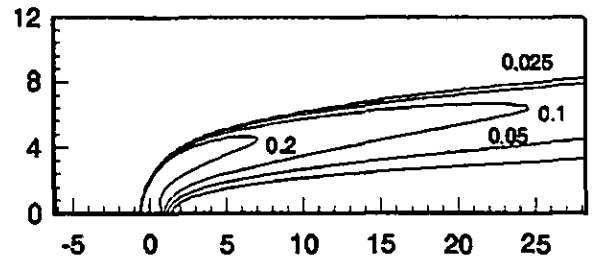

9(e) Sc=0.8

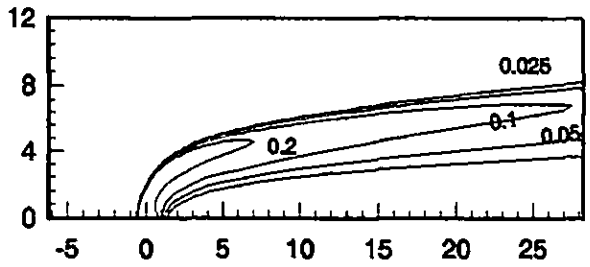

9(f) Sc=1.2

Fig. 9 Non-dimensional temperature distribution in the symmetric plane (J=8, H/D=12).

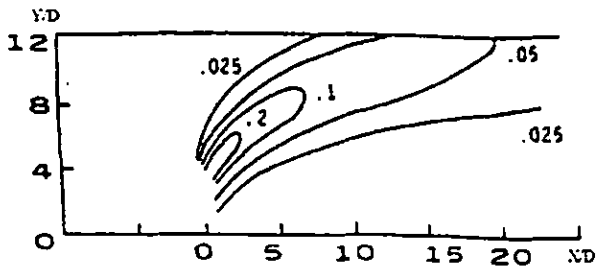

10(a) Experimental data

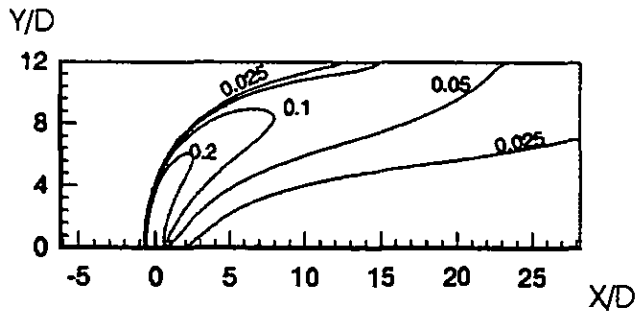

10(b) Sc=0.2

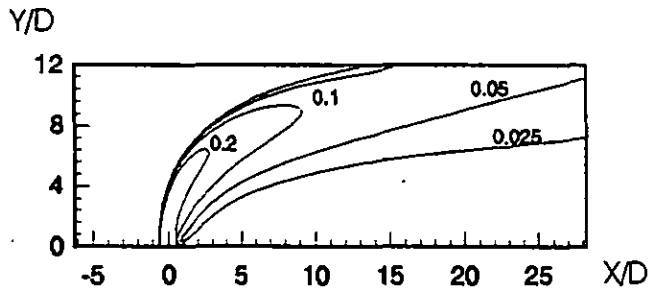

10(c) Sc=0.3

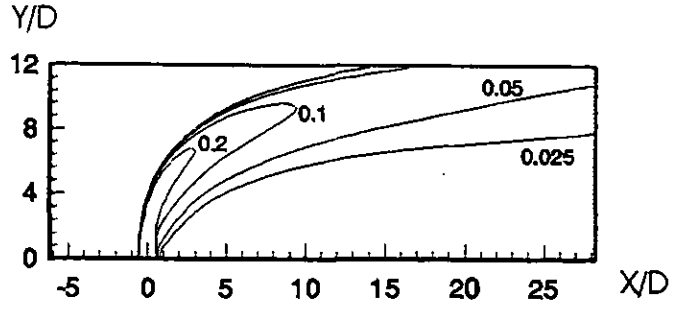

10(d) Sc=0.5

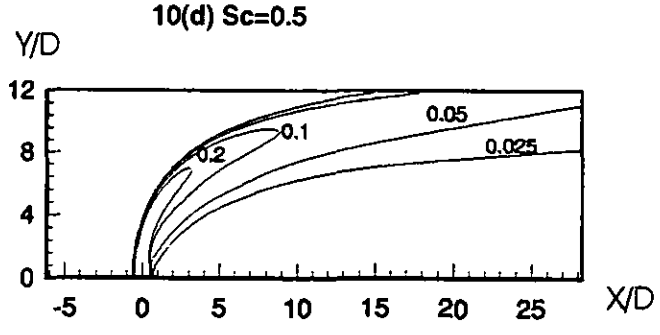

10(e) Sc=0.7

Fig. 10 Non-dimensional temperature distribution in the symmetric plane (J=32, H/D=12).

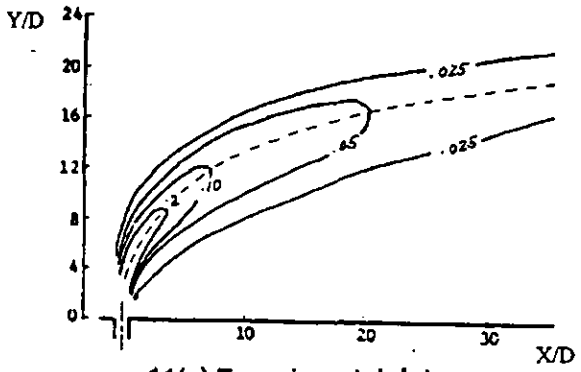

11(a) Experimental data

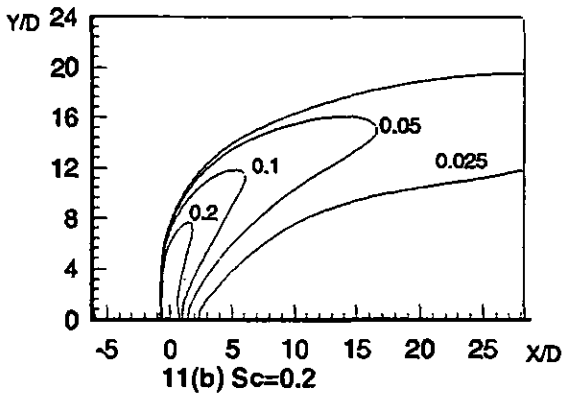

11(b) Sc=0.2

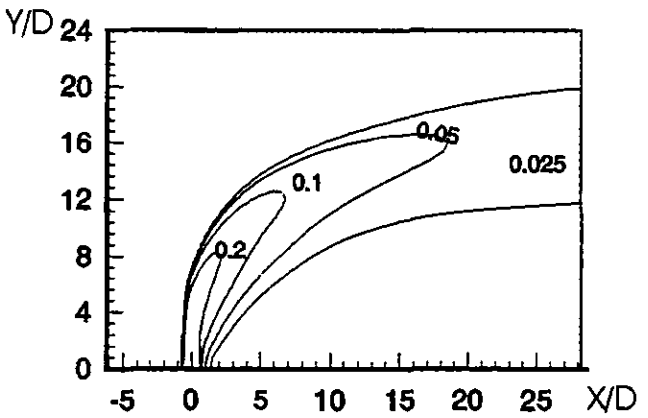

11(c) Sc=03

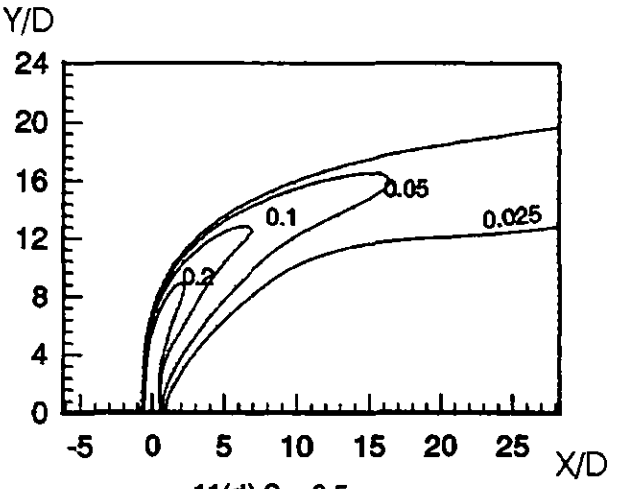

11(d) Sc=0.5

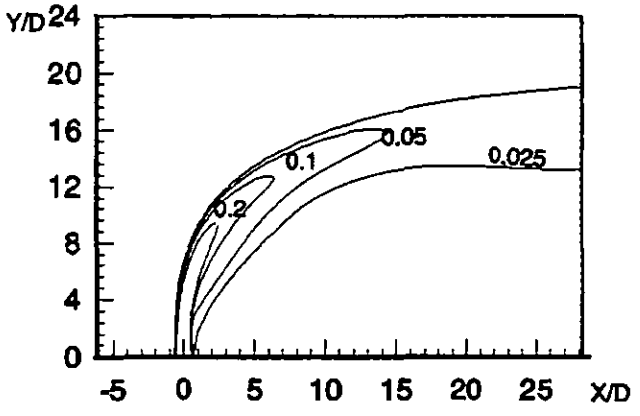

11(e) Sc=0.8

Fig. 11 Non-dimensional temperature distribution in the symmetric plane (J=72, H/D=24).